

# Modulation transfer function characterization and modeling of a Scophony infrared scene projector

Eric F. Schildwachter, MEMBER SPIE

Martin Marietta  
P.O. Box 555837  
Orlando, Florida 32855

Glenn D. Boreman, MEMBER SPIE

University of Central Florida  
Department of Electrical Engineering  
Center for Research in Electro-Optics and Lasers  
Orlando, Florida 32816

**Abstract.** A Scophony-configuration infrared scene projector, consisting of a raster-scanned CO<sub>2</sub> laser and an acousto-optic (AO) modulator, was characterized for modulation transfer function (MTF) performance. The MTF components considered in the model were the Gaussian beam input to the AO cell, the finite aperture of the scan mirror, the width of the detector in the image plane, the transfer function of the amplifier electronics, and a term caused by Bragg-angle detuning over the bandwidth of the amplitude modulation (AM) video signal driving the AO cell. The finite bandwidth of the input video signal caused a spread in the Bragg angle required for maximum diffraction efficiency. In the Scophony configuration, a collimated laser beam enters the AO cell at only one particular angle, so a falloff of diffraction efficiency (and hence MTF) resulted as the modulation frequency was increased. The Bragg-angle detuning term was found to dominate the measured system MTF.

*Subject terms:* infrared imaging systems; infrared scene projector; Scophony; hardware-in-the-loop simulation; scene generation; modulation transfer function; acousto-optics.

*Optical Engineering* 30(11), 1734-1738 (November 1991).

## CONTENTS

1. Introduction
2. Scene projector configuration
3. Subsystem MTF models
  - 3.1. Scophony scanner MTF
  - 3.2. Detector and amplifier MTF
  - 3.3. Comparison with measured system MTF
  - 3.4. Bragg-angle detuning MTF
4. Conclusion
5. Acknowledgment
6. References

## 1. INTRODUCTION

Infrared (IR) scene projection is a useful tool for hardware-in-the-loop simulation. The performance of entire seeker systems, including the detectors, can be characterized without the need of field trials. However, the IR scene projector must be capable of better performance than the systems to be tested. One important aspect of system performance is modulation transfer function (MTF). We find that a major MTF component of a Scophony IR scene projector results from Bragg-angle detuning of the acousto-optic (AO) cell.

## 2. SCENE PROJECTOR CONFIGURATION

The Scophony scene projector seen in Fig. 1 performs a two-dimensional raster scan of a CO<sub>2</sub> laser beam ( $\lambda = 10.6 \mu\text{m}$ ) that is intensity modulated in response to an amplitude modulation (AM) video signal, which drives the AO cell. The AM video signal consists of a high-frequency carrier wave, with modula-

tion at lower frequencies. The AO cell produces Bragg diffraction from the phase grating caused by spatially periodic variations of refractive index. A lens follows the AO cell to produce a Fourier transform plane at the polygon scanner. Each diffracted order consists of a central spot corresponding to the acoustic carrier frequency, surrounded by the spectrum of the modulation signal. The zeroth diffracted order is blocked, and the first diffracted order is retransformed by another lens to produce an irradiance distribution in the image plane, corresponding to the modulating waveform in the AO cell. Because of the double Fourier-transform operation, the AO cell and the image plane are conjugate to one another, at a magnification determined by the two focal lengths. The carrier frequency of the acoustic AM

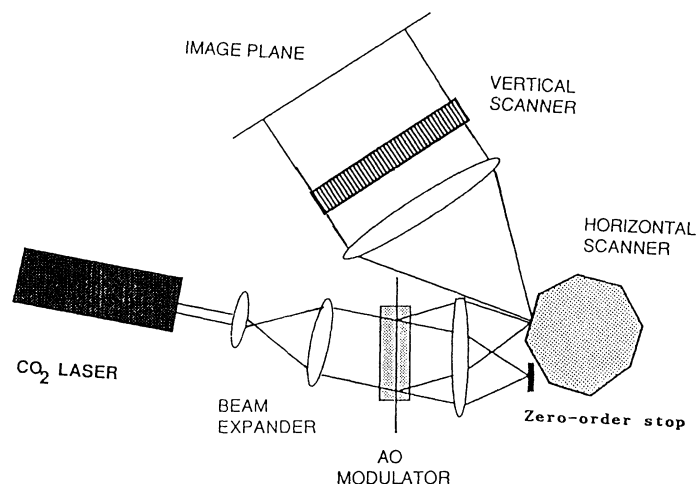


Fig. 1. Schematic of the Scophony IR scene projector.

Invited paper IR-018 received May 7, 1991; revised manuscript received June 28, 1991; accepted for publication July 1, 1991.

© 1991 Society of Photo-Optical Instrumentation Engineers.

waveform corresponds to dc in the image plane, while the modulating acoustic signal produces the irradiance variation.

To keep our analysis general, we have cast our MTF models and measurements in terms of acoustic frequency. For any particular projector configuration, the acoustic frequency can be converted to image-plane spatial frequency, provided that the optical magnification and the acoustic velocity are known.

Light entering the AO cell at the Bragg angle  $\Theta_B$  exits in either the zeroth or the first diffracted order, as seen in Fig. 2. The Bragg angle is defined as

$$\Theta_B = \sin^{-1}(\lambda f / 2v) , \quad (1)$$

where  $\lambda$  is the wavelength of the radiation in air,  $f$  is the acoustic frequency, and  $v$  is the velocity of sound in the AO cell material. The spatial grating period of the acoustic wave inside the AO cell is  $\Lambda = v/f$ . The spatial frequency  $\xi$  of the phase grating is the inverse of  $\Lambda$ :

$$\xi = f/v . \quad (2)$$

In our experiments, the carrier frequency  $f_c$  of the information on the AO cell was 40 MHz, and the sound velocity in the germanium cell material was 5506 m/s, producing a Bragg angle of 2.2 deg, and a grating spatial frequency  $\xi = 7.25$  cycles/mm for the carrier wave.

In a classic flying-spot scanner, the laser beam is focused into a small region of the AO cell, so that the modulation produced will have a fast rise time. This produces a single point in the image plane that is scanned in two dimensions to produce the desired scene.

In the Scophony scanner,<sup>1-4</sup> the input laser beam is collimated to fill a large portion of the AO cell aperture. By spreading the laser beam across the aperture, several picture elements of the image are contained in the traveling acoustic wave in the AO cell at any instant in time. Illumination of a larger portion of the AO cell in the Scophony projector results in a slower rise time, but with a higher spatial resolution, as compared with the flying-spot method. Since the information associated with any given picture element moves across the AO cell with the acoustic velocity, the corresponding resolution element in the image plane would move also, unless that motion were compensated. The compensation is provided by the motion of the horizontal scan mirror. The rotation velocity of the polygon is adjusted such that the final image is stationary.

The scanner system used the following component values. The aperture of the AO cell was 12 mm horizontal by 8 mm

vertical. The beam expander was anamorphic, producing an elliptical Gaussian beam profile, with full widths at the  $1/e^2$  level of irradiance of 4.4 mm horizontal and 3.0 mm vertical. This resulted in a larger flux throughput for the AO cell, without affecting the horizontal resolution of the projector. The polygon scanner was placed at the focus of the lens that followed the AO cell ( $F = 652$  mm). The 24-sided polygon had a horizontal facet dimension  $A = 6.75$  mm. The angular velocity was 656 rev/s.

### 3. SUBSYSTEM MTF MODELS

The MTF of the scene projector system can be modeled as the product of the MTFs of the following individual subsystem components: Scophony scanner, detector, amplifier, and the AO cell.

#### 3.1. Scophony scanner MTF

The polygon scanner is in the Fourier transform plane of the AO cell. The radiation that eventually forms the final image is contained in the first diffracted order. For a carrier of acoustic frequency  $f_c$ , sinusoidally AM modulated at an acoustic frequency  $f_m$ , the irradiance distribution consists of three Gaussian spots, as seen in Fig. 3(a). The three frequency components in the AM waveform are  $f_c$ ,  $f_c + f_m$ , and  $f_c - f_m$ , which are related to spatial frequencies  $\xi_c$ ,  $\xi_c + \xi_m$ , and  $\xi_c - \xi_m$  by Eq. (2).

Using Gaskill's<sup>5</sup> notation, each of the individual horizontal amplitude profiles is the Fourier transform of the Gaussian amplitude beam profile  $\alpha \text{Gaus}(x/b)$  that illuminated the AO cell. Using the Fourier transform relationship

$$\alpha \text{Gaus}\left(\frac{x}{b}\right) \xrightarrow{\mathcal{F}} \alpha|b| \text{Gaus}(b\xi) , \quad (3)$$

we have for the Fourier transform amplitude  $a(\xi)$  at the facet plane:

$$a(\xi) = \alpha|b| \text{Gaus}(b\xi) * \left\{ \delta(\xi_c) + \frac{1}{2}[\delta(\xi_c + \xi_m) + \delta(\xi_c - \xi_m)] \right\} . \quad (4)$$

Each spot is located at a distance  $x$  from the optical axis of the transform lens,<sup>6</sup> which depends on the particular spatial frequency of interest in the AO cell, the wavelength of the radiation, and the lens focal length:

$$x = \xi \lambda F = \frac{f \lambda F}{v} . \quad (5)$$

Using the change of variables  $\xi = x/\lambda F$ , we obtain the amplitude profile in the facet plane as a function of position  $x$ :

$$a(x) = \alpha|b| \text{Gaus}\left(\frac{xb}{\lambda F}\right) * \left\{ \delta\left(\frac{x_c}{\lambda F}\right) + \frac{1}{2} \left[ \delta\left(\frac{x_c + x_m}{\lambda F}\right) + \delta\left(\frac{x_c - x_m}{\lambda F}\right) \right] \right\} . \quad (6)$$

Modulation at higher frequencies produces spot positions farther from the carrier spot location, which are eventually truncated by the polygon facet, as shown in Fig. 3(b). Thus, the finite

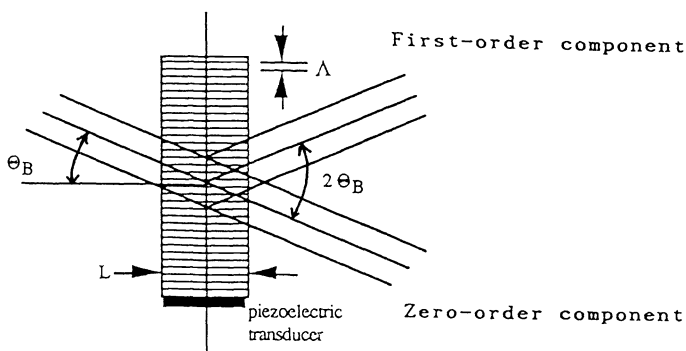


Fig. 2. Bragg diffraction configuration.

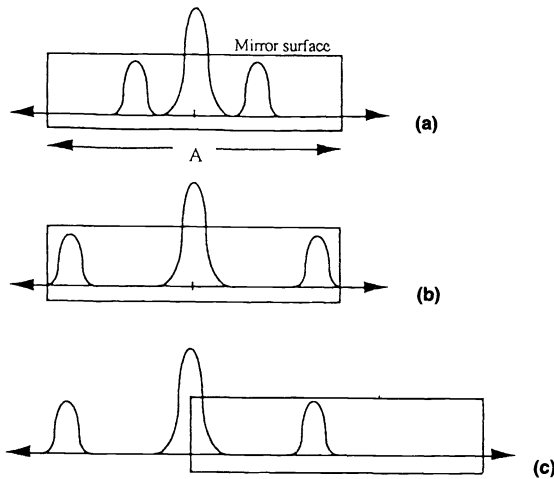


Fig. 3. (a) Irradiance distribution at the facet plane. (b) Truncation resulting from increased modulation frequency. (c) Single-sideband configuration.

facet dimension  $A$  of the scanner acts as a low-pass filter, limiting the spatial frequencies present in the final image.

Figure 3(c) shows how the frequency passband of the Scophony scanner can be doubled by using a single-sideband (SSB) configuration.<sup>4</sup> We used this configuration in our setup. Using Eqs. (3) through (6), we can easily establish  $f_{\text{limit}}$ , the cutoff modulation frequency of the scanner for spots having delta function profile. In terms of spot position:

$$x_c - x_{\text{limit}} = \frac{\lambda F}{v} (f_c - f_{\text{limit}}) = A, \quad (7)$$

yielding

$$f_{\text{limit}} = f_c - \frac{Av}{\lambda F} \quad (8)$$

in terms of acoustic frequencies for the SSB case. Using our system parameters, Eq. (8) gives a cutoff frequency of 5.4 MHz.

Relaxing the assumption of a delta function spot profile, we see from Eq. (6) that the spot profiles at the facet will be of finite extent. In this case the cutoff will not be abrupt;  $f_{\text{limit}}$  in Eq. (8) will be the frequency at which the center of the spot crosses the facet edge.

As the modulation frequency increases, the Gaussian spot corresponding to  $f_c$  (dc in the image) will maintain a constant position on the facet. Given a constant dc level in the image, the MTF of the SSB Scophony scanner subsystem is the amount of power from the spot corresponding to  $f_m$  that is contained within the facet (and thus reaches the image plane), as a function of  $f_m$ . The calculation will need the Gaussian spot profile expressions in terms of irradiance rather than amplitude, and will incorporate the usual normalization to unity at low spatial frequencies.

As stated previously, the laser beam illuminating the AO cell had a horizontal full width at  $1/e^2$  in irradiance of 4.4 mm. Since the Fourier transform relationship between the AO cell and the facet plane is in terms of amplitude, we must express the incident beam in those terms. Continuing with the notation of Ref. 5, an amplitude function

$$u(x) = \alpha \text{Gaus}(x/b) = \alpha \exp \left[ -\pi \left( \frac{x}{b} \right)^2 \right] \quad (9)$$

corresponds to an irradiance function

$$I(x) = |\alpha|^2 \text{Gaus} \left( \frac{\sqrt{2}x}{b} \right). \quad (10)$$

Thus our input beam in amplitude terms was  $\alpha \text{Gaus}(x/b)$ , with  $b = 3.9$  mm. Using Eq. (5), we find that

$$\alpha|b| \text{Gaus}(b\xi) = \alpha|b| \text{Gaus} \left( \frac{bx}{\lambda F} \right) = \alpha(3.9 \text{ mm}) \text{Gaus} \left( \frac{x}{1.67} \right), \quad (11)$$

yielding an irradiance profile

$$I(x) = \alpha^2(3.9 \text{ mm})^2 \exp \left[ -\pi \left( \frac{\sqrt{2}x}{1.67} \right)^2 \right], \quad (12)$$

with a 0.94-mm half-width at the  $1/e^2$  level of irradiance.

Thus, we can write an expression for the MTF:

$$\text{MTF}(\xi_m) = 1 - \frac{\int_A^\infty I(x - \xi_m \lambda F) dx}{\int_A^\infty I(x) dx}, \quad (13)$$

which, using our system parameters, yields the curve seen in Fig. 4. This calculation is equivalent to the truncation ratio method used in Ref. 3, but has the advantage of a specific functional description for the MTF.

### 3.2. Detector and amplifier MTF

The finite width of the detector gives another MTF component for the system. The 100- $\mu\text{m}$  width in the spatial domain corresponds to an averaging interval  $\tau$  in the time domain, which will have a sinc MTF contribution:

$$\text{MTF}_{\text{det}}(f) = \frac{\sin \pi \tau f}{\pi \tau f}. \quad (14)$$

To calculate  $\tau$ , we proceed as follows. The 24-facet polygon rotates at 656 rev/s. The rate is thus 15,744 facets/s. This pro-

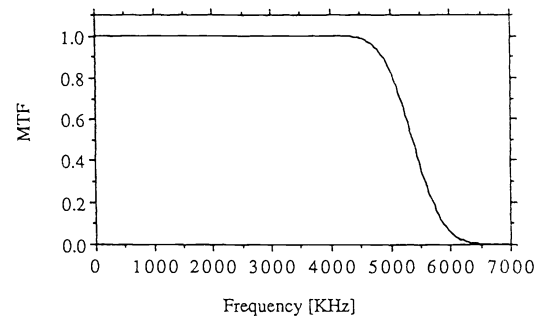


Fig. 4. MTF for Scophony scanner subsystem.

duces a line-scan time of  $63.5 \mu\text{s}$ , as required by standard video. Each facet is  $15 \text{ deg}$ , equivalent to  $30 \text{ deg}$  of beam scan. The detector is placed at a distance of  $650 \text{ mm}$  from the scanner. The  $30 \text{ deg}$  of beam scan will cover a spatial distance of  $650 \text{ mm} \times \tan 30 \text{ deg}$ , or  $375 \text{ mm}$ . This  $375 \text{ mm}$  is covered in  $63.5 \mu\text{s}$ , yielding a linear scan velocity of  $5905 \text{ m/s}$ . The  $100\text{-}\mu\text{m}$  detector width is thus equivalent to a  $17\text{-ns}$  averaging interval. The first zero of the sinc-function MTF associated with that averaging would occur at  $59 \text{ MHz}$ . This MTF is essentially constant over the frequencies of interest. Using Eq. (14), we obtain  $\text{MTF}_{\text{det}}$  of  $0.976$  at  $7 \text{ MHz}$ .

The amplifier electronics has a transfer function that constitutes another MTF component. The amplifier used was measured to have the transfer function seen in Fig. 5. This subsystem MTF was measured with a sine-wave signal generator. MTF was simply the output modulation depth seen, given a constant input modulation depth.

### 3.3. Comparison with measured system MTF

In our measurements of the MTF of the projector, we drove the AO cell with video signals consisting of the  $40\text{-MHz}$  carrier, amplitude modulated with sinusoids of different frequencies. Since we were primarily concerned with horizontal resolution, the vertical scan mirror shown in Fig. 1 was removed. We also removed the lens following the polygon scanner, and placed a  $100\text{-}\mu\text{m}$ -wide HgCdTe detector (at liquid nitrogen temperature)  $650 \text{ mm}$  from the polygon. Thus, we expanded the scale of the fringes corresponding to any particular frequency (compared to keeping the original image-plane location), and eliminated the need for a discrete aperture (which would have had to be cooled to  $77 \text{ K}$ ) in front of the detector. The scan velocity of the polygon was adjusted slightly to yield fringes that moved across the detector. The maximum and minimum values of the sinusoidal irradiance at each frequency were recorded as the fringes scanned past the detector, from which the MTF was calculated.

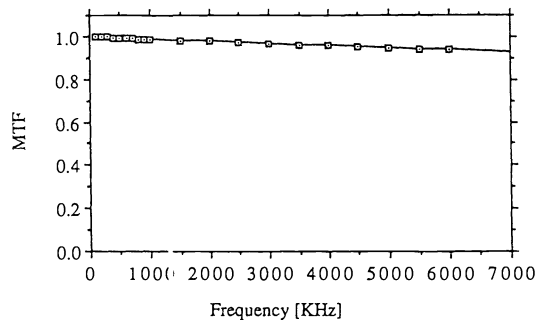


Fig. 5. Measured MTF of electronics subsystem.

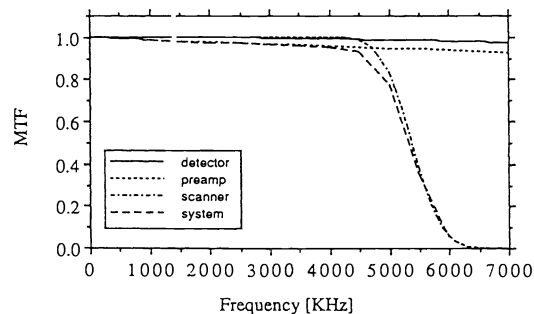


Fig. 6. Predicted system MTF, exclusive of Bragg-angle detuning.

Figure 6 shows the product of the MTFs of the subsystems considered so far, along with the individual components for the Scophony scanner, the detector, and the preamp. Figure 7 compares this MTF product with the system MTF actually measured. Obviously, an additional term must be included in the model. The MTF term presented in Sec. 3.4 accounts for the variation of diffraction efficiency with modulation frequency. With that additional component included, our MTF model will predict the measured MTF more closely.

### 3.4. Bragg-angle detuning MTF

The AM video signal that was input to the AO cell contained a  $40\text{-MHz}$  sinusoidal carrier, with sinusoidal modulation frequencies  $f_m$  to  $7 \text{ MHz}$ . The Bragg angle expressed in Eq. (1) depends on the acoustic frequency. The projector system was tuned for maximum power throughput at the  $40\text{-MHz}$  carrier wave (dc in the image). In the SSB configuration, when the carrier wave is AM modulated by a sinusoid of frequency  $f_m$ , the resulting spectrum consists of two delta functions:  $\delta(f_c)$  and  $\delta(f_c + f_m)$ . Since in the Scophony configuration the laser radiation is collimated and enters the AO cell at one particular angle, the radiation is not simultaneously at the Bragg angle for both the carrier and the modulating signal. When adjusted for maximum diffraction efficiency at the carrier frequency, the diffraction efficiency falls off<sup>2,7</sup> as a function of modulation frequency as follows:

$$\eta(\psi) = \left[ \frac{\sin(\pi L \psi f_c / v)}{\pi L \psi f_c / v} \right]^2, \quad (15)$$

where  $L$  is the width of the acoustic beam (assumed to be uniform, as seen in Fig. 2) perpendicular to the direction of propagation. The attenuation of the beam in the direction of propagation is not included in the above expression. The variable  $\psi$  is the mismatch of Bragg angles:

$$\psi = \sin^{-1} \left[ \frac{\lambda(f_c + f_m)}{2v} \right] - \sin^{-1} \left( \frac{\lambda f_c}{2v} \right). \quad (16)$$

Combining Eqs. (15) and (16), we obtain the diffraction efficiency as a function of modulation frequency  $\eta(f_m)$ . Since the dc image term corresponding to the carrier has  $\eta = 1$ , we find that the MTF component attributable to Bragg detuning is simply  $\eta(f_m)$ , plotted in Fig. 8. This component will multiply the MTFs of the other subsystems, the product of which was seen as the upper curve in Fig. 7. The effect of Bragg detuning dominates,

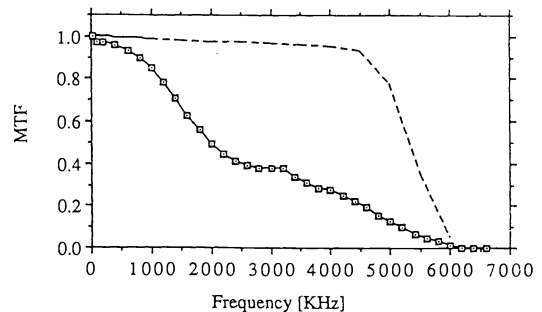
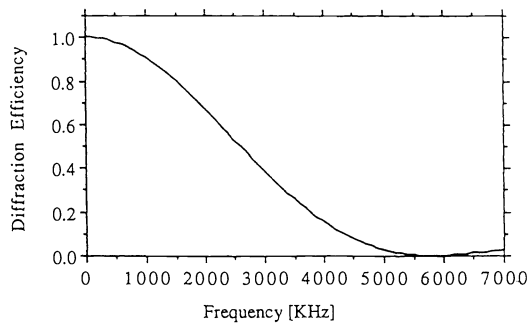
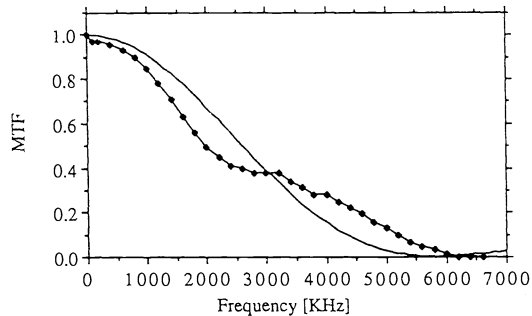


Fig. 7. Predicted system MTF, exclusive of Bragg-angle detuning (top curve); measured system MTF (bottom curve).



**Fig. 8. Diffraction efficiency versus modulation frequency: the MTF resulting from Bragg-angle detuning.**



**Fig. 9. Predicted system MTF, with all terms included (solid curve); measured system MTF (dotted curve).**

and largely determines, the overall system MTF curve. Figure 9 compares the product of all the MTF components considered to the measured system MTF curve, with good agreement.

#### 4. CONCLUSION

An infrared scene projector based on the Scophony scanner was characterized for MTF performance. The major component of the system MTF was found to be the detuning of the Bragg angle from the finite bandwidth of the AM video signal. The residual variation between the model presented and the MTF measurements might result from the nonuniformity of the acoustic field inside the AO cell in both transverse and longitudinal directions, since these effects are not included in the present model.

#### 5. ACKNOWLEDGMENT

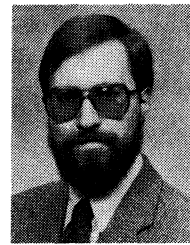
This work was supported by the Florida High Technology and Industry Council and by the Martin Marietta Graduate Fellowship Program. We gratefully acknowledge the loan of the projector from the Naval Training Systems Center, Orlando, Florida.

#### 6. REFERENCES

1. D. M. Robinson, "The supersonic light control and its application to television with special reference to the Scophony television receiver," *Proc. IRE* 27, 483-486 (1939).
2. A. Korpel, R. Adler, P. Desmares, and W. Watson, "A television display using acoustic deflection and modulation of coherent light," *Proc. IEEE* 54, 1429-1437 (1966).
3. R. V. Johnson, "Scophony light valve," *Appl. Opt.* 18, 4030-4038 (1979).
4. R. V. Johnson, J. Guerin, and M. E. Swansberg, "Scophony spatial light modulator," *Opt. Eng.* 24, 83-100 (1985).
5. J. Gaskill, *Linear Systems, Fourier Transforms, and Optics*, pp. 47, 421, Wiley, New York (1978).
6. J. Goodman, *Introduction to Fourier Optics*, p. 85, McGraw-Hill, New York (1968).
7. M. G. Cohen and E. J. Gordon, "Acoustic beam probing using optical techniques," *Bell Syst. Tech. J.* 44, 693-721 (1965).



**Eric F. Schildwachter** received his BS degree in engineering sciences from the University of Florida in 1985 and his MS degree in electrical engineering from the University of Central Florida in 1991. He has been employed at Martin Marietta Missile Systems in Orlando, Florida, since 1985 and is presently involved in the design and evaluation of both ground-based and space-borne sensor systems. He is a member of SPIE.



**Glenn D. Boreman** received his BS degree in optics from the University of Rochester in 1978 and his Ph.D. degree in optical sciences from the University of Arizona in 1984. He has held visiting technical staff positions at ITT, Texas Instruments, U.S. Army Night Vision Laboratory, and McDonnell Douglas. Dr. Boreman has been at the University of Central Florida since 1984 and is currently an associate professor of electrical engineering. He is a member of OSA, IEEE, SPIE, and SPSE and is a past president of the Florida section of OSA.